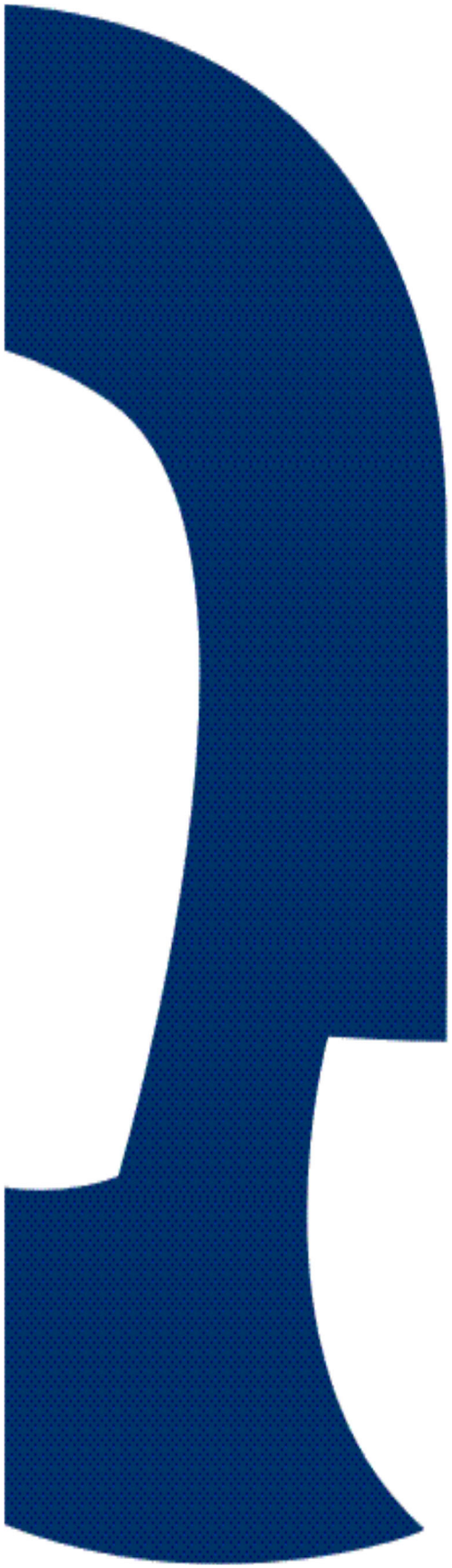

Master Interuniversitario en Oceanografía

FACULTAD DE CIENCIAS DEL MAR

UNIVERSIDAD DE LAS PALMAS DE GRAN CANARIA

Spatio-Temporal Variability of the Bransfield Current System (Antarctica)

Marta Veny López

2019/2020

Máster Universitario en Oceanografía

Tutores:

Mª de los Ángeles Marrero Díaz

Borja Aguiar González

Grupo de Investigación:

OFYGA-Departamento de Física

SPATIO-TEMPORAL VARIABILITY OF THE BRANSFIELD CURRENT SYSTEM (ANTARCTICA)

Marta Veny López

Máster Universitario en Oceanografía, Universidad de las Palmas de Gran Canaria

Tutores: Mª de los Ángeles Marrero Díaz,
Borja Aguiar González

Grupo de investigación: OFYGA – Departamento de Física

17/07/2020

Alumna Tutores

Fdo: Marta Veny Fdo: Ángeles Marrero Fdo: Borja Aguiar

ACKNOWLEDGMENTS

To Dr. Ángeles Marrero Díaz and Dr. Borja Aguiar González, supervisors of this study, for their rigorousness, support and guidance along the project development and for trusting me to carry this work out. Thank you for dedicating your time to teach me and giving me the opportunity to receive all your knowledge. It has been a pleasure.

Also, I'm grateful to my family and friends, who have always encouraged me to go on. You all are always my best relief and company.

This work has been supported by the Spanish government (Ministerio de Economía y Competitividad) through project FLUXES (CTM2015-69392- C3-3- R).

INDEX

ABSTRACT

The Bransfield Strait is a semi enclosed region located between the Antarctic Peninsula and the South Shetland Islands (SSI), where the most distinctive feature of the circulation is a baroclinic jet flowing northeastward along the southern slope of the SSI, the Bransfield Current (BC; Niiler et al., 1991). Recent studies have shown that the BC propagates as a buoyant gravity current, recirculating around the north-eastern tip of the islands while shedding an anticyclonic eddy (Sangrà et al., 2011, 2017). However, most previous works are based on summertime measurements and a more comprehensive spatio-temporal view of the regional circulation is still lacking to further understand the governing shelf dynamics.

In this study we provide the first year-round description of the Bransfield Current based on an extensive dataset of direct velocity measurements. These measurements were routinely collected along ship tracks from 275 cruises between 1999 and 2014. From these observations, a climatological database has been developed to examine the seasonal variability of the BC. Results support the BC is a recurrent feature of the circulation in Bransfield Strait, flowing northeastward all along the southern slope of the SSI not only during summer but also during spring and autumn. We note that winter data scarcity prevents us from a similar statement during this season but still enables the confirmation of a strong northeastward-flowing current at least south off Nelson Island. Lastly, the recirculation of the BC around the northeasternmost tip of the SSI also appears apparent in all seasons but during winter due to lack of data and its fate is, therefore, yet to be confirmed in the future.

Key words: South Shetland Islands, Bransfield Current System, Spatio-Temporal Variability, Direct Velocity Measurements

RESUMEN

El Estrecho de Bransfield es una región semi-cerrada situada entre la Península Antártica y las Islas Shetland del Sur (SSI), donde la característica más singular de la circulación es una corriente baroclina que fluye al noreste a lo largo del talud sur de las SSI, la Corriente de Bransfield (BC; Niiler et al., 1991). Estudios recientes muestran que la BC se propaga como una corriente de gravedad, recirculando a lo largo del extremo noreste de las islas y formando un remolino anticiclónico en su recirculación hacia el norte, al oeste de la Isla Rey Jorge (Sangrà et al., 2011, 2017). Los estudios previos están basados en medidas realizadas durante el verano, por lo que se desconoce la persistencia de la BC a lo largo del año y su posible variabilidad espacio-temporal.

En este estudio, se presenta la primera descripción estacional de la Corriente de Bransfield, basada en un extenso conjunto de datos de velocidad obtenidos con SADCP. Las medidas se tomaron de forma sistemática siguiendo las rutas de desembarco en bases antárticas durante 275 cruceros que tuvieron lugar entre 1999 y 2014. Los resultados corroboran que la BC es una particularidad recurrente de la circulación en el Estrecho de Bransfield, que fluye hacia el noreste a lo largo del talud sur de las SSI no solamente en verano, sino también en primavera y otoño. La escasez de datos en invierno no permite precisar la misma descripción, aunque se ha podido constatar la presencia de un corriente circulando hacia el noreste en el sur de la Isla Nelson. Por último, la recirculación de la BC al oeste de la Isla Rey Jorge también aparece en todas las estaciones, excepto en invierno debido a la falta de datos, y su dirección requiere ser confirmada en un futuro.

Palabras clave: Islas Shetland del Sur, Sistema de Corrientes de Bransfield, Variabilidad Espacio-Temporal, Medidas de Velocidad Directas.

1. INTRODUCTION

The Antarctica is the southernmost continent on Earth and it is surrounded by the "Southern Ocean", whose northern limit reaches as far as the northernmost presence of the Antarctic Circumpolar Current (ACC), which have been reported at about 30-38ºS (Talley et al., 2011). The ACC connects the major basins located at the Pacific, Atlantic and Indian Oceans, coupling these waters to the rest of the ocean circulation. The ACC is composed of a series of narrow jets flowing to the east around the continent (clockwise) maintained by westerly winds. It is only restricted in the Drake Passage by the Antarctic Peninsula (AP) and the South Shetland Islands (SSI) (Figure1). It is also altered because of mid-ocean ridges (Talley et al., 2011). The ACC connection among ocean basins accounts for the Southern Ocean influence on the global climate, sea level, and marine ecosystems (Rintoul et al., 2018).

Antarctic features are also altered, varying around the Antarctic region and triggering different consequences and scenarios such as the extent of sea-ice platforms. The stability of these platforms depends on variability of atmospheric temperature (Mulvaney et al., 2012) and wind impacts (Hendry et al., 2018), among other variables. Thus, El Niño-Southern Oscillation and Southern Annular Mode also have impacts on sea ice cover, inducing year-to-year changes (Talley et al., 2011). Rintoul et al. (2018) showed an atmospheric and oceanic warming and, therefore, a response of sea ice covers. The response is characterized by a loss ratio of Antarctic mass which will cause a sea level rise in the next centuries, exceeding 5 mm/year in sea level terms.

The mentioned changes are noticeable at the West Antarctic Peninsula (WAP), which is a sensitive region to the global change (Rintoul et al., 2018). For instance, Rintoul et al. (2018) have already reported that WAP sea ice platforms may be melting, causing an irreversible collapse. Specifically, the south of the AP is one of the Earth regions that is heating up faster (Mulvaney et al., 2012).

However, the Bransfield Strait (BS), which is our study area, show different trends due to its particular hydrographic and dynamic features (Henley et al., 2019), based on summer data.

The BS is a semi enclosed region, situated between the AP and the SSI, divided into Western, Central and Eastern basins which are separated by sills characterized by depths of 1000 m. Based on summertime data, some studies have stablished a basic circulation pattern (Grelowski et al., 1986; Hoffmann et al., 1996; Zhou et al., 2006), with western and eastern inflows into the BS. The western inflow is characterized by a warmer and fresher water coming from the Bellingshausen Sea, the Gerlache Strait and the Circumpolar Current which circulates north-eastwards along the northern portion of the Strait. Meanwhile, the eastern inflow is distinguished by colder and saltier water from the Weddell Sea flowing south-westwards along the southern half of the Strait. Tokarczyk (1987) concluded that the western and eastern inflows can gradually change and García

et al. (1994) named the water masses associated to these currents as Transitional Zonal Water with Bellingshausen influence (TBW) and Transitional Zonal Water with Weddell Sea influence (TWW) (Figure 1).

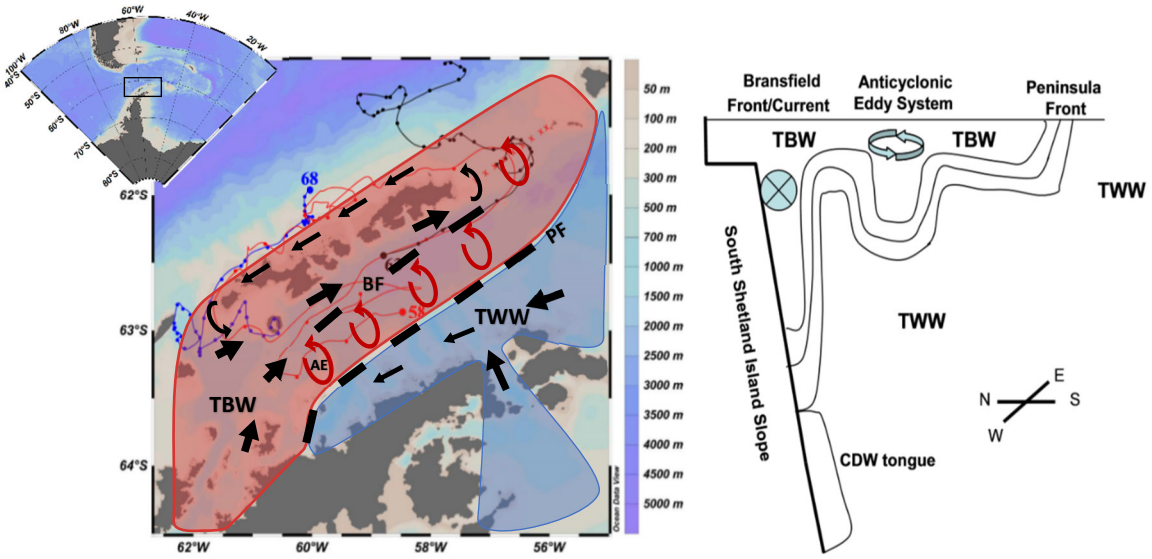

Figure 1. Regional map of the circulation pattern and components of the Bransfield Current System (BCS): a) horizontal structure scheme modified from Sangrà et al. (2017) where blue and red lines are drifter trajectories of their study; b) BC vertical structure scheme and water masses distribution (Sangrà et al., 2011).

According to these summertime descriptions, TBW is the overlying well-stratified and relatively warm and fresh water. It occupies a narrow surface band at the eastern part and reaches deeper depths near the SSI at the western basin (Sangrà et al., 2011). According to Basterretxea and Arístegui (1999) and Sangrà et al. (2011), TBW is seasonally originated at Bellingshausen Sea and Gerlache Strait due to summer heating and ice melting leading to warmer and fresher surface TBW during middle summer than during earlier summer. More recently, also based on summertime data, Sangrà et al. (2017) defined the Bransfield Current System (BCS), with the identification of TBW also north of the SSI, whose recirculation scheme is shown in Figure1a. Regarding to TWW, this is the homogeneous and colder and saltier water which occupies nearly the main body of the eastern basin of the Strait as well as the other BS basins (Grelowski et al., 1986; Hoffmann et al., 1996; García et al., 2002; Zhou et al., 2002).

As part of the current system described above, two frontal zones are present in this Strait, both separating TBW and TWW (García et al., 1994; López et al., 1999): the Peninsula Front (PF) and the Bransfield Front (BF). Parallel to these fronts, and all along the BS, a street of mesoscale anticyclonic eddies (AEs) with TBW characteristics also appears as a recurrent feature of the summertime circulation (Figure 1b). The PF is about 10 km wide and is located at the central and eastern basins, from the surface and down to 100 m, thus defined as a mesoscale shallow structure. The PF is closer to the AP being no longer present at the western part of the central basin (Sangrà et al., 2011). Differently, the BF, defined as a deeper front along the SSI, is a subsurface TBW front described at depths around 50 to 400 m up to the SSI slope (Niiler et al., 1991; García et al., 1994). Generally, the BF has a wider range than the PF extending from 10 to 20 km. The BF is wider and

shallower at the western section than at the eastern one, but the front reaches the surface in both sections (Sangrà et al., 2011).

Between the BF and the SSI, one finds the Bransfield Current (BC) (Niiler et al., 1991; Zhou et al., 2002, 2006). The BC is a baroclinic jet characterised by a buoyant less-dense TBW, which flows northeastward over denser TWW. Initially, both Niiler et al. (1991) and Zhou et al. (2002, 2006) defined the BC as a wind-driven induced current. However, Sangrà et al. (2011, 2017) and Poulin et al. (2014) found that the BC propagates as a buoyant gravity current along the SSI slope over being constrained in a narrow coastal band by the Coriolis force and by the buoyancy-induced pressure gradient. The BC is distinguished for its 20 km width and a central jet velocity of 0.3-0.4 m s^{-1} at the surface, decaying linearly towards the bottom and being narrower and more intense in the eastern end (Zhou et al., 2002, 2006; Savidge and Amft, 2009). According to Sangrà et al. (2017), the northeastward geostrophic transport (0-500 db) is 0.8 Sv along the SSI slope. Once the BC reaches the SSI tip, the trajectory describes an anticlockwise circulation around the SSI tip transporting 0.7 Sv (Figure 2). Afterwards, 0.14 Sv of this current are recirculated south-westward along the northern section of the SSI into the Drake Passage to complete the circulation of the BC around the SSI. Off the BC, the transport is weaker and variable (Sangrà et al., 2011).

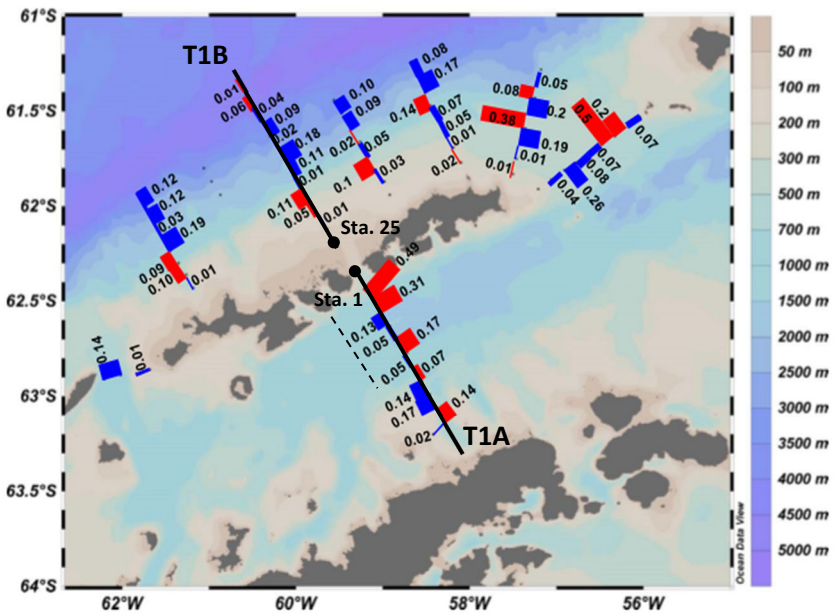

Figure 2. Map of positive (red) and negative (blue) geostrophic cross-transects transports (Sv) integrated from 0 to 500 db. Modified from Sangrà et al., 2017. The continuous black line indicates the position of transects 1A and 1B. The black dots indicate the numbered stations of study transects closer to the SSI. The discontinuous black line indicates the position of the transect in Morozov (2007) study (see Figure 4).

Following the description above, the BC can be described as a coastal gravity current that recirculates generating a dynamic structure as seen in Figure 3 (Sangrà et al., 2017). Figures. 3a, 3b and 3c show that the colder (< -0.45ºC), saltier (> 34.45), denser (> 27.64 kg m^{-3}) and almost homogeneous TWW occupy the main body of the Strait. Meanwhile, TBW overlie TWW, occupying a narrow vertical band along the southern SSI slope and

reaching depths of 400 m. As compared to TWW, TBW are warmer (> -0.4ºC), fresher (< 34.35), less-dense (< 27.64 kg m^{-3}) and well-stratified (Sangrà et al., 2017).

The limit between TBW and TWW is complex to define. The salinity pattern is the most similar to the density distribution, which is much related to the geostrophic dynamics. However, the tongue of CDW (Circumpolar Deep Water) is not distinguished in Figure 3c (potential density anomaly). This CDW can be clearly observed as a warm nucleus at depths of 350 m leaning on the southern SSI slope (Figure 3a). This nucleus is also shown in Figure 3b as CDW are saltier than TBW. Considering all these figures and value ranges of the indicated parameters, the subsurface core of the BC has a maximum depth not deeper to 300 m (S < 34.35).

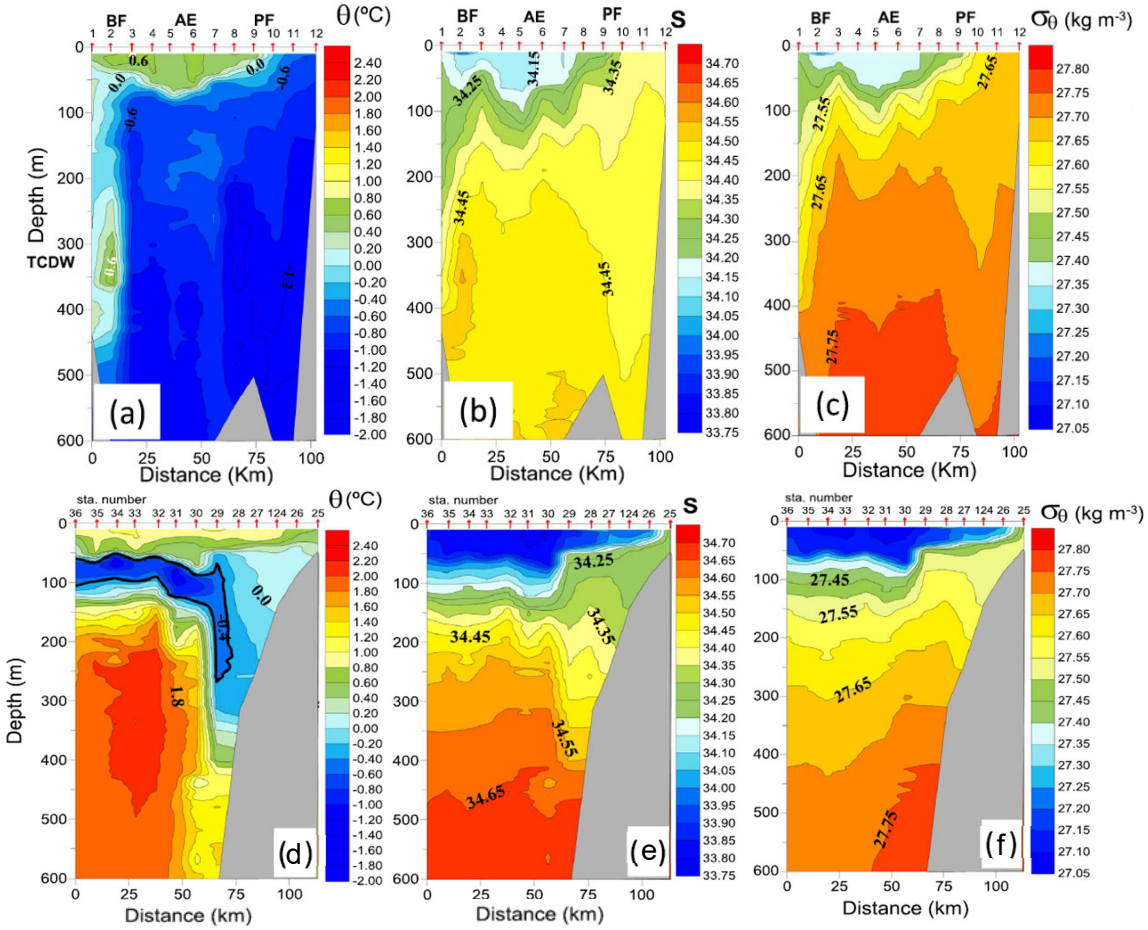

Figure 3. Vertical profiles of (a) potential temperature, (b) salinity and (c) density anomaly along transect T1A; and (d) potential temperature, (e) salinity and (f) density anomaly along transect T1B. Figure from Sangrà et al. (2017).

The recirculation of TBW from the BS to the northern SSI slope is shown in Figures 3d, 3e and 3f. These waters occupy vertical regions of characteristic potential temperature (-0.4ºC < θ < 0.4ºC), salinity (34.0 < S < 34.4) and potential density anomaly (27.4 kg m^{-3} < σ_θ < 27.64 kg m^{-3}) (Sangrà et al., 2017). The temperature and salinity structures are significantly different comparing surface stations at the northern shelf of the SSI and deeper stations, located at depths higher than 300 m. At the surface, waters present TBW

characteristics due to the BC recirculation. This recirculation water flows at shallow depths at the stations near the coast (st. 25 and 26), but it turns into a subsurface water when it reaches the northern slope, at a maximum depth around 200 m. Above these recirculation waters, we observe Antarctic Surface Water (AASW), described with a salinity minimum. Beneath AASW, WW (Winter Water) occupies a subsurface layer (marked with a bold black line in Figure 3a). At the deepest region, below WW, the water column is occupied by Upper Circumpolar Deep Water (UCDW). The UCDW is separated from the SSI slope waters and WW by the southern boundary of the ACC, known as "Coastal Water Boundary" or Scotia Front (García et al., 2002).

To the best of our knowledge, only one previous work reported observations of the BC vertical structure based on direct velocity measurements collected during spring (Morozov, 2007). Figure 4 presents these observations based on from Lowered Doppler Profilers (LADCP) measurements from a transect perpendicular to the Greenwich Island. In this transect, the core of the BC flows northeastward forming a wedge shape at velocities up to 45 cm/s in the upper 250 m.

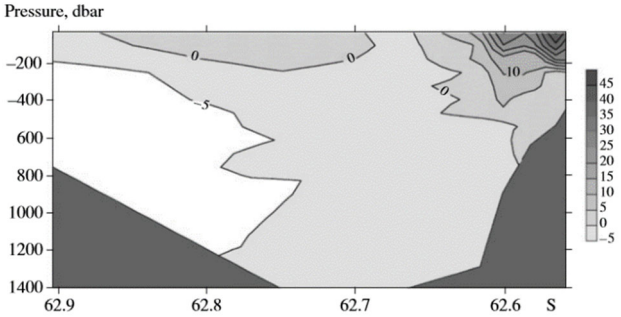

Figure 4. Vertical section of LADCP velocities in Bransfield Strait (see position in Figure 2). Positive values correspond to the northeastward direction. Figure from Morozov, 2007.

The aim is to characterize the seasonal variations of the Bransfield Current System. Upon data availability, first estimates of seasonal volume transports are also discussed. We have structured this work in different sections. In Section 2, we describe data and methods. In Section 3, we present our results following three subsections: first, the horizontal distribution of the velocity field; second, its vertical structure; and third, the volume transport driven by the BC. In Section 4, we discuss the variability of the BC system. Section 5 presents the main conclusions. Lastly, in Section 6, we outline the first steps of future work based on these data.

2. DATA AND METHODS

This study is based on an extensive dataset of direct velocity measurements collected with Shipboard Acoustic Doppler Current Profilers (SADCP) (https://www.nodc.noaa.gov/). SADCP releases sound waves that scatter back from water column particles and measures the current velocities based on the Doppler effect of the waves. These measurements were obtained from routinely ship tracks from 275 cruises between 1999 and 2014, covering all the seasons. The database contains 130.280 profiles with 102 different depth levels

from 30 to 1040 m. The barotropic tidal signal has been removed using CATS2008 (Circum-Antarctic Tidal Simulation) (Padman et al., 2002).

To carry out this study, we did the following steps: organize the database, analyze its feasibility for the temporal variability studies and obtain climatological variables for the analysis of the seasonal variability. Then, we generated horizontal distribution maps of the velocity at different depth levels. Also, we obtained the vertical profiles of the horizontal velocity components and plot their vertical. Finally, we calculated the integrated volume transport from 30 to 250 m. All these steps are described in detail in the following methodology subsections.

2.1. EXPERIMENTAL DESIGN FOR THE DATABASE

The database was collected from cruises that repeat certain tracks at the Antarctica region, usually for logistic operations. These data can be downloaded, organized and labelled depending on the purpose of the work. As the first part of this study, the dataset is organized to have a wider application than the needed for this thesis.

2.2. DATA AVAILABILITY FOR TEMPORAL VARIABILITY STUDIES

Taking into account the characteristics of the database, the data distribution is not uniform neither in space nor in time. There are not permanent stations so, for variability studies that are based on averages, the generation of a data grid is helpful. After testing some grid resolutions, data is finally binned into 10x10 km cell grids of horizontal resolution along and across the Strait. The 10x10km grid resolution is a compromise between the gain of enough data falling within each grid cell and the retention of mesoscale structures, since in this region the Rossby radius is on the order of 10 km (Chelton et al., 1998). Larger grid cells would make data available in all cells, but the structure of the mesoscale would be lost. On the other hand, smaller grids would allow a better understanding of the local velocity field, but the signal would be noisier and without spatial continuity, as a significant number of cells might not have any data at all.

We assign a correlative grid cell number to our grid (see Figure 5) to be able to quickly locate grid cells of high data density for studies of time variability. The cells are identified from number 1 to 6419, but Figure 5 only shows a part of all the dataset cells. The cell number assignment starts at the northwesternmost study region becoming higher to the northeast in the same row. Once the numbering finishes the row, it continues in the first column of the next row. Cells without numbering respond to the lack of data. However, the number is kept to include dataset extension, if there is any in the future.

Once the data is gridded, we focus the study on the BS region and obtain, for every cell, averaged variables at different temporal scales. Therefore, we construct the climatological dataset of velocities that we use in this study. We follow the scheme of average step by step, summarized in Figure 6. This process results in averaged variables at different temporal scales, for every cell, in all depth levels in which data are available.

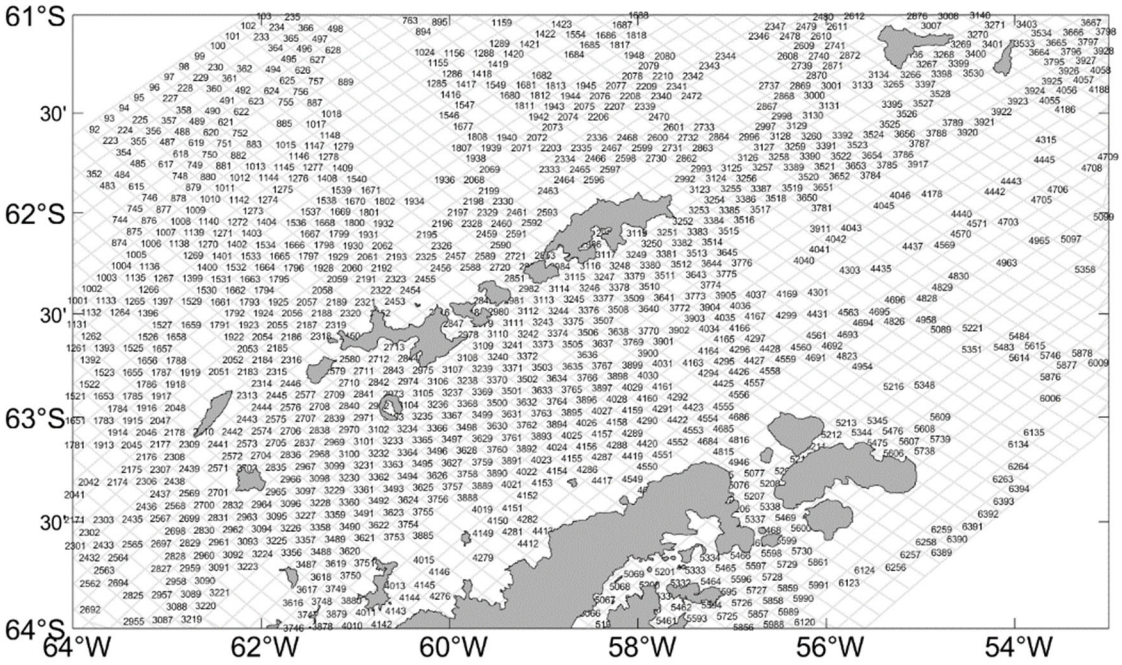

Figure 5. Map of grid cell numbers which represents the identification of each cell that contain vertical velocity profiles around the SSI.

The first step is to average the available velocity profiles in each cell for every month of each year. In the second step, we obtain the variables that correspond to the seasonal average of each year, taking into account the three monthly averaged profiles of every year. The months considered for every season are: Summer (January, February and March data), Autumn (April, May and June data), Winter (July, August and September data) and Spring (October, November and December data). In step 3, we obtain the climatological seasonal profile in every cell based on the seasonal average of every year. All these steps allow both do a climatological study and studies of interannual seasonal variability. As the fourth step, and completing the climatological dataset, we obtain the average monthly climatological profiles in every cell, starting with the monthly averages of every year acquired in step 1.

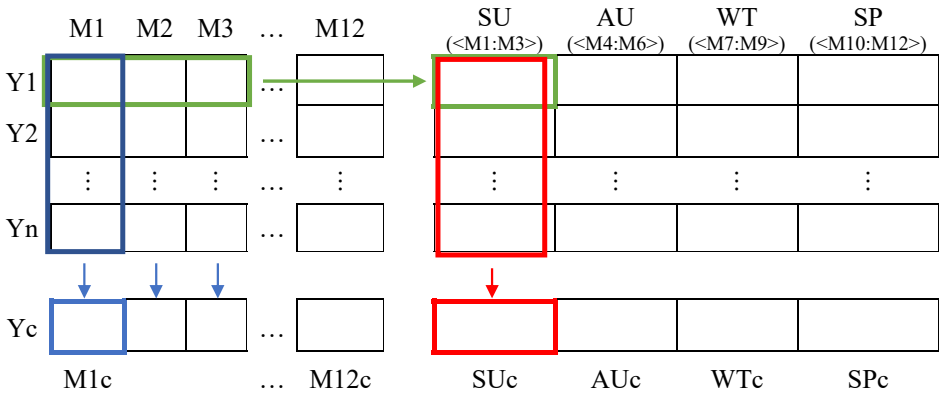

Figure 6. Scheme for the generation of the climatological variables with the following codes: M#: the monthly averaged variable of the month #; Y#: the year for which the averaged variables are obtained; SU, AU, WT and SP: seasonal averages for year Y# of Summer, Autumn, Winter and Spring, respectively; M#c: climatological average of the month #; SUc, AUc, WTc and SPc: seasonal climatological averages.

The number of profiles that are available in each cell also allows us to know the statistical accuracy of the possible variability studies. Already focused on the BS region, we represent the maps of seasonal data density (Figure 7). The number of profiles represents the number of available seasonal profiles (i. e., a number of 5 within the grid cell of a summer data density map means there are 5 summer profiles from different years).

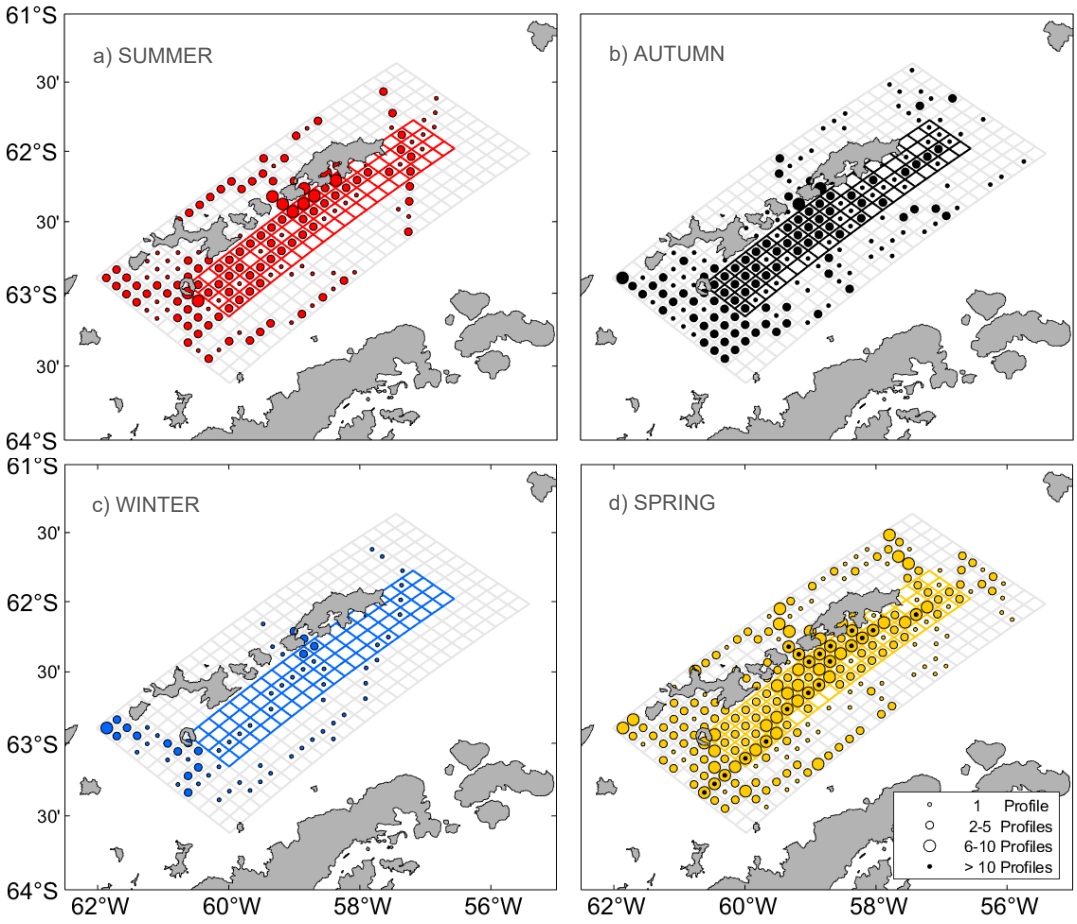

Figure 7. Maps of seasonal data density (see legend) which represent the amount of velocity profiles in each cell around the SSI. Grid cells highlighted in colours show the along-shelf and cross-shelf transects selected for this work.

2.3. REPRESENTATION OF VELOCITY FIELDS

Velocity horizontal distributions are analyzed from 50 to 250 m. This representation eases the identification of the transects that contain data down to depths of 250 m. To accomplish the aim of this study, we select the velocity horizontal distribution at 150 m (Figure 8) as the BC is usually present at those depths, according to the reviewed bibliography. The velocity vectors are shown with coloured arrows according to the vector magnitude, orientated to the direction of the current. These horizontal sections are also used to select the transects of interest which have enough amount of data.

The vertical distributions of these transects are also investigated. To represent the vertical distribution of the u and v components of the velocity, we average seasonal data (already

monthly averaged). Because the vertical profiles we use have different reaching-depths, the averaging process requires ad hoc depth ranges. Since the vertical profiles can reach different depths, we analyze the profiles of each transect cell to average until the last common depth. The change of depth from one profile to another would cause a misleading velocity profile (i.e., if one profile reaches down to 250 m and the other one reaches down to 300 m, the averaged result presents a velocity step between those depths).

2.4. HORIZONTAL TRANSPORT

We calculate volume transport taking into account the velocities in the water column and the area covered. These transects contain data in 90% of the section as required to represent the vertical sections. The condition is needed to have significantly representative sections.

The total volume transport is defined as

$$U(t) = \int_0^L \int_{-h(x')}^{-h_0(x')} u\,(x', z, t) dz dx',$$

where L is the transect length (m), h_0 is the depth of the shallowest velocity value, h is the depth of deepest velocity considered, u is the east velocity component and x' is the coordinate along de transect. The values of h_o and h depend on the profile, but usually, in this work, their values are 30 m and 250 m respectively. The transects considered in this study are 20 km length. This volume transport is expressed in Sverdrup (Sv)

In addition, to analyze seasonal changes in the Bransfield Current, the horizontal transport vector has been obtained. In this work, the components of the horizontal transport vector have been defined as the integrated value of u and v components between h_o and h, in each seasonal average profile. This horizontal transport is expressed in m^2/s.

3. RESULTS

Through this section we aim to determine whether the BC is a year-round feature of the circulation in Bransfield Strait and whether this current displays significant seasonal variations in both its horizontal and vertical structure as well as volume transport capacity.

For clarity, the results are organized under the following three subsections. In Section 3.1, we characterize the seasonal horizontal pattern of the Bransfield Current System at a selected depth. In Section 3.2, we characterize the spatial and seasonal vertical pattern of the BC following a series of transects nearly perpendicular to both the BC and the coastline of the SSI. Lastly, in Section 3.3, we provide the first seasonal estimates of the volume transport (Sv) and the horizontal transport carried out by the BC (m^2/s), both based on direct velocity measurements.

3.1. HORIZONTAL DISTRIBUTION OF THE BRANSFIELD CURRENT. SEASONAL VARIATIONS

Figure 8 shows the horizontal circulation patterns of the velocity field varying seasonally at a selected depth (150 m), where the core of the BC is expected from previous works (Morozov, 2007; Sangrà et al., 2011, 2017). Vectors are unitary and display their magnitude following shades of colours (see colorbar). The data coverage corresponds to the data density shown in Figure 7.

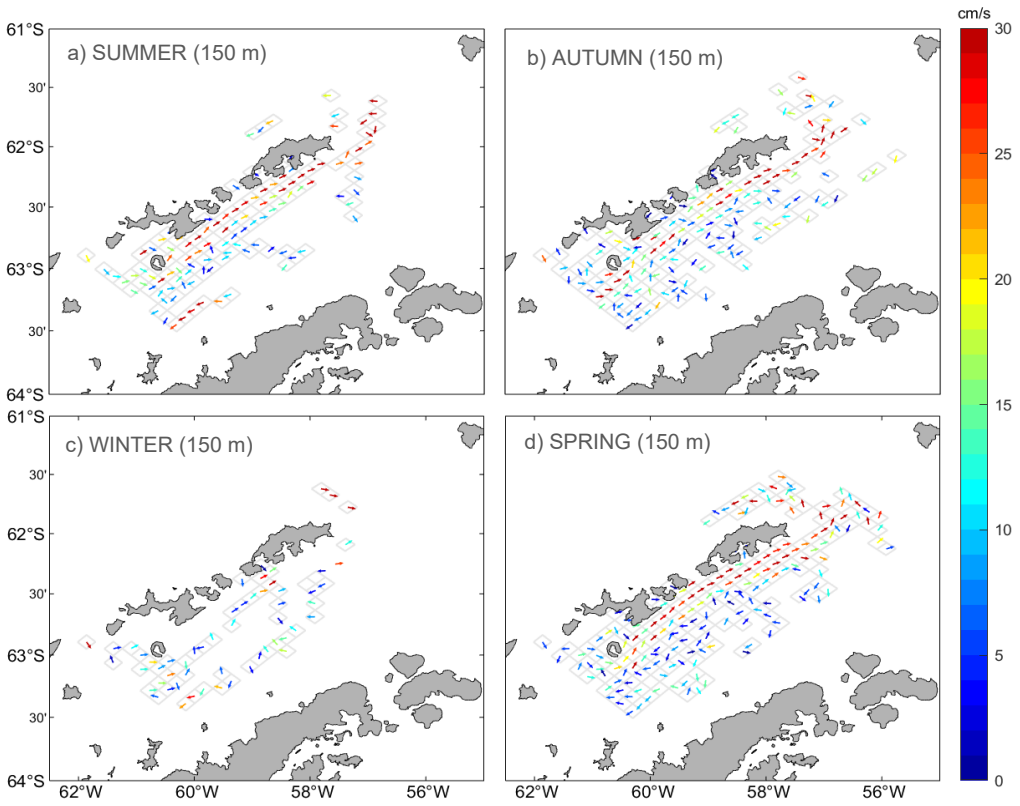

Figure 8. Seasonal maps of the horizontal velocity field at 150 m for: a) Summer, b) Autumn, c) Winter, and d) Spring. The velocity field is represented with unitary vectors showing the direction of the current, coloured according to the velocity magnitude.

The most outstanding feature is the recurrence of a northeastward-flowing jet along the southern coastline of the South Shetland Islands. We attribute this signal to the BC, likely transporting TBW, and which is visible from Deception Island to King George Island in all seasons but in winter. During winter, scarcity of data hampers the view of the full domain but allows us to confirme the presence of the BC from Greenwich Island to King George Island.

As expected, the core of the BC, characterized by higher velocities, is found within the grid cells closer to the coast. This supports that the BC flows as a gravity current hugging the island slopes and following the bathymetry. Also, we note that the width of the jet changes spatially along its pathway; it narrows from Greenwich-Robert Islands to Nelson Island and widens downstream towards King George Island.

Seasonally, the strength of the BC varies. From spring to summer, the BC flows as a relatively strong (~30 cm/s) and continuous jet. During autumn, the jet weakens from Deception Island to Robert Island, strengthening again downstream from this location. In winter, relatively high velocities about 30 cm/s are only found, upon data availability, south off Nelson Island.

Importantly, the recirculation of the BC turning around King George Island is noticeable for all seasons but winter. During this season there are just not enough data to reveal a conclusive statement about the recirculation of the BC.

Lastly, we note a weaker flow of wider extent is also present within Bransfield Strait, flowing southwestward. We attribute this signal to the Weddell Sea Inflow, likely transporting TWW. The remaining vectors not aligned to any of the currents mentioned above and occupying the middle of the Strait might be the street of anticyclonic eddies reported in Sangrà et al. (2011, 2017).

3.2. VERTICAL PATTERN OF THE BRANSFIELD CURRENT. SEASONAL VARIATIONS

A series of transects (T6, T10, T11 and T12) have been selected (see locations of the transects in Figure 9) to analyze the summertime spatial variability of the BC along its full path, i.e. along the southern slope of the SSI (Figure 10).

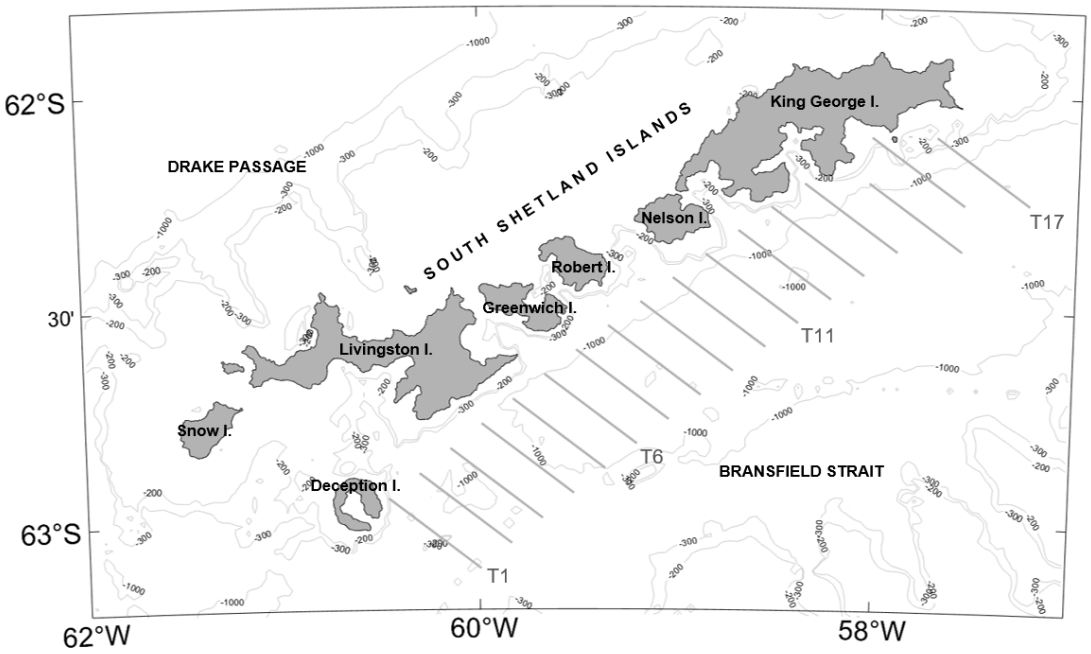

Figure 9. Map showing the transects of study based on the gridded domain over Bransfield Strait and adjacent areas.

Regarding its summertime vertical structure, there is a clear pattern for when the BC flows either at the wake of islands or at channels between islands. This is visible by comparison of transects 6 and 11, which show the BC at the wake of Livingston and Nelson Islands, with transects 10 and 12, which show the BC at channels between SSI. In transects 6 and 11, the core of the BC leans on the island slope, while in transects 10 and 12 the core moves offshore due to the jet flowing parallel to channels between islands.

In terms of current strength (Figure 10, left-panels), the zonal component of the velocity flows at about 35 cm/s through both transects 6 and 10, when hugging the island slope. Differently, in transects 10 and 12, while at the channels between SSI, we find the core of the BC displays both weaker (30 cm/s) and higher velocities (45 cm/s), respectively, than in previous transects. Following the bathymetry, the meridional component (Figure 10, right-panels) reaches highest velocities (~25 cm/s) in transect 6.

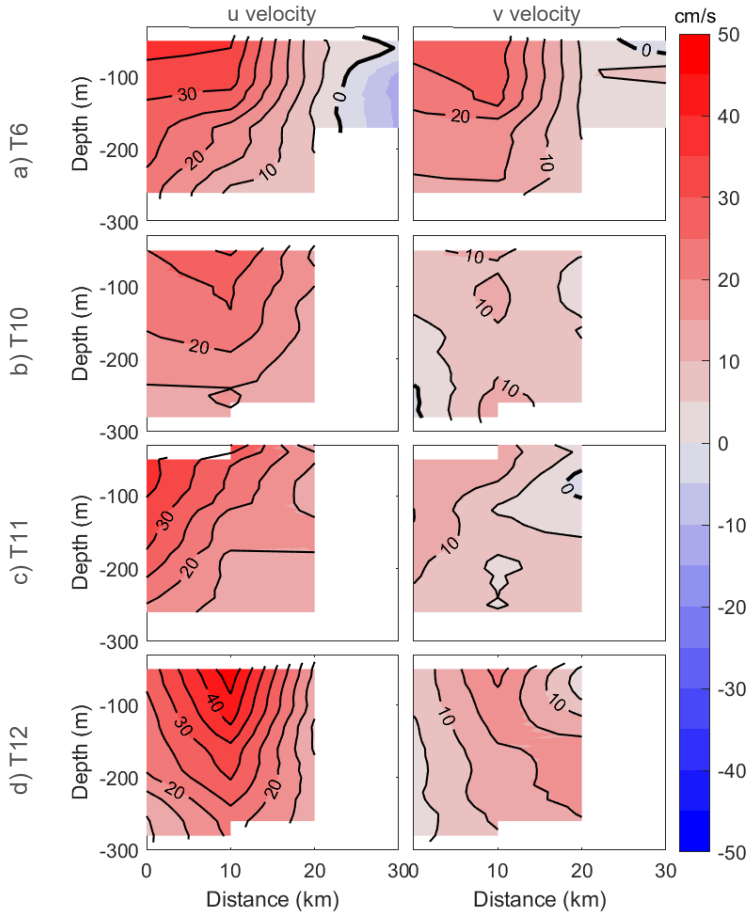

Figure 10. Vertical sections of a SADCP-based climatologies for u and v velocity components during summer of transects: a) T6, b) T10, c) T11 and d) T12 (see Figure 9). Distance starts at the southern SSI slope being perpendicular to the islands. Note that velocity is positive to the east (u velocity) and north (v velocity); i.e., in the direction of the BC. Conversely, negative velocities show southwestward flows. Blank regions are due to scarcity of data.

Through Figure 11 we characterize the seasonal variability of the vertical structure of the BC. The major finding is the presence of a strong and recurrent jet, the BC, flowing towards the east next to the island slopes. Additionally, during autumn and spring, data

density allows us to also visualize a counterflow, flowing towards the west, and likely driven the Weddell Sea Inflow. These two panels (Figure 11 b and d) are suggestive of the Bransfield Front holding the BC as a baroclinic jet and opposing the Weddell Sea Inflow.

In terms of shape and strength, some other features are of interest about the core of the BC in Figure 11. From spring to autumn, the core appears hugging the slope of Nelson Island while the core detaches from the slope during winter. Also, it is during autumn and winter when the core reaches its highest velocities (~35 cm/s).

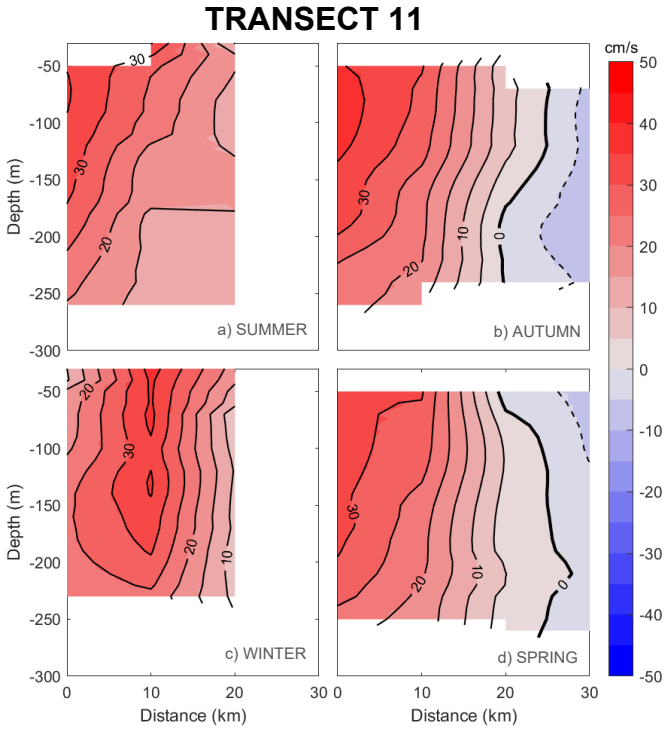

Figure 11. Vertical sections of a seasonal climatology for zonal velocities in transect 11, based on SADCP measurements (see T11 in Figure 9) during: a) Summer, b) Autumn, c) Winter and d) Spring. Distance starts at the southern SSI slope being perpendicular to the islands. Note that velocity is positive to the east; i.e., in the direction of the BC. Conversely, negative velocities show westward flows. Blank regions are due to scarcity of data.

Figure 12 presents the vertical structure of the BC in a similar fashion as done in Figure 11 but now for transects 10 and 12 instead of transect 11. The vertical structure of the BC in all vertical sections (Figures 11 and 12) agrees well with the view of a surface baroclinic jet whose velocities decrease at depth, especially from 200-250 m towards deeper waters. This baroclinic pattern is also visible in horizontal maps of the velocity field at different depths (see Appendix, Figures 15-18).

The shape and strength of the BC also change by seasons. In transects 10 and 12 (Figure 12), where the core of the current is located offshore while flowing at channels between islands. In these cases, the core of the BC presents its highest velocities above 50 cm/s

during autumn (transect 10), and above 30 cm/s and 45 cm/s during summer and autumn (transect 12), respectively. In spring, the core of the BC weakens (20-30 cm/s) and appears to move inshore towards the bathymetry between islands for both transects 10 and 12.

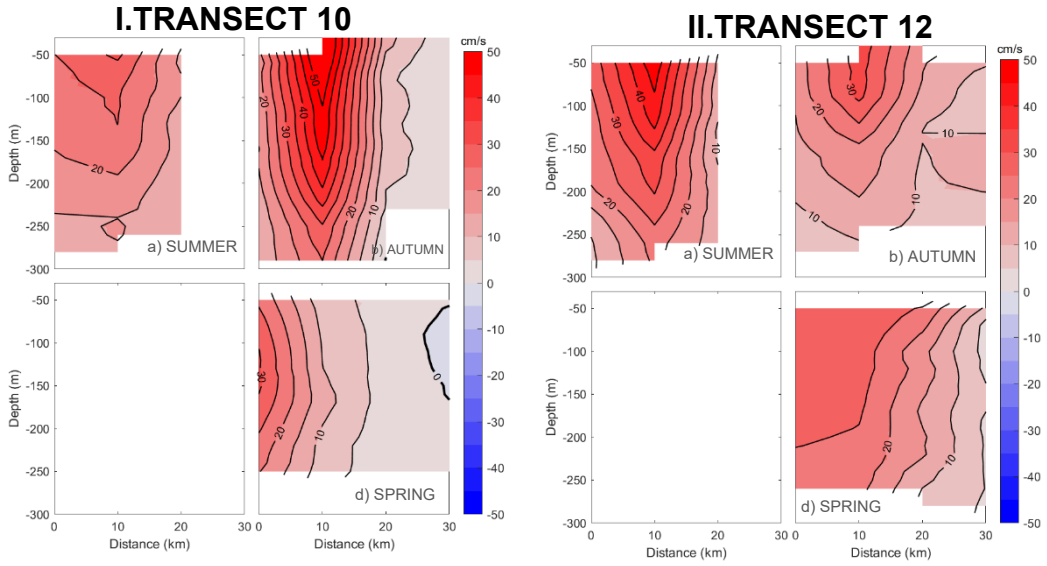

Figure 12. Vertical sections of a seasonal climatology for zonal velocities in transects I) 10 and II) 12, based on SADCP measurements during: a) Summer, b) Autumn, c) Winter and d) Spring. Distance starts at the southern SSI slope being perpendicular to the islands. Note that velocity is positive to the east; i.e., in the direction of the BC. Conversely, negative velocities show westward flows. Blank regions are due to scarcity of data.

3.3. HORIZONTAL TRANSPORT. SEASONAL VARIATIONS

In this section we investigate the spatial and seasonal variability of the horizontal transport driven by the Bransfield Current from the shallowest depth level available (30 m) down to 250 m.

Before computation of transport estimates and because data coverage is, on occasions, different among vertical profiles of velocity measurements, we have imposed a threshold of 90% data coverage for any given profile. This threshold ensures that horizontal transports are estimated only when at least 90% of the data are present, what leads to more robust and reliable comparisons. Also, this condition accounts for the lack of transport estimates for winter, where scarcity of vertical profiles is the largest (see Figure 7c).

Accordingly, Table 1 presents the seasonal estimates of the net (eastward) volume transport (U in Sv) driven by the BC at each transect shown in Figure 9; note that the transects of study are nearly perpendicular to the island coastlines and to the stream direction of the Bransfield Current. Spatially, these estimates indicate that the highest volume transports occur for all seasons downstream of Robert Island (U ranges from 0.46-1.38 Sv from transect 8 to 17) and, especially, before the BC approaches the turning point

for the recirculation around the SSI, where U ~ 0.75-1.14 at transects 14 to 17. From Deception Island to Greenwich Island (transects 1 to 7) averaged values of the volume transport from Table 1 are: 0.72 Sv during summer, 0.46 Sv during autumn and 0.53 Sv during spring.

Table 1. Estimates of net (eastward) volume transport (Sv) for transects 1-17 based on direct velocity measurements. Volume transport is integrated from 30 to 250 m depth, beginning at the SSI slope to 20 km offshore. Positive (negative) values mean eastward (westward) transport. See the transects of study in Figure 9.

	Summer, U (Sv)	**Autumn, U (Sv)**	**Winter U (Sv)**	**Spring, U (Sv)**
T1	0.50	-	-	0.43
T2	-	0.32	-	0.55
T3	0.75	0.64	-	0.63
T4	0.96	0.72	-	0.64
T5	-	0.42	-	0.30
T6	0.91	0.30	-	0.58
T7	0.46	0.34	-	0.56
T8	0.86	0.43	-	0.57
T9	-	0.65	-	0.48
T10	0.89	1.38	-	0.52
T11	0.93	0.90	1.01	0.85
T12	1.16	0.76	-	1.06
T13	-	-	-	0.95
T14	1.03	-	-	0.75
T15	-	-	-	1.36
T16	-	-	-	-
T17	-	-	-	1.14

Seasonally, the volume transport estimates in Table 1 indicate that, generally speaking, nearly all transects present their highest values both during spring and summer. One outstanding exception occurs at the transect 10 during autumn, where the BC reached its highest volume transport on record (U = 1.38 Sv) upon data availability. Regarding to winter, we can only confirm the presence of a remarkably high volume transport of 1.01 Sv at the transect 11.

Lastly, Figure 13 presents on a map the transects of study along with their associated seasonal horizontal transports (m^2/s). The four vectors along each transect originates from averaging the horizontal transport (m^2/s) driven by all available profiles within each of the four grid cells closest to the island coastlines. The magnitude of the velocity field is scaled to the vector in the upper left corner of each panel.

In agreement with results in Figure 8, the distribution of the horizontal transports over the BC domain show higher values closer to the coast and decreasing offshore, especially during summer and spring. This structure supports further the jet-like nature of the BC hugging the slope while following the bathymetry. The latter feature is especially noticeable when the BC starts its turn around the King George Island. During autumn, it seems the core of the BC either widens or moves offshore along the pathway of the BC.

This is especially clear at transects 3, 5, 10, 12, 13 and 14. Finally, during winter, the available data provide estimates that suggest the BC is not only strong but also wider, as compared to other seasons, at transect 11.

As it occurred to the velocity field pattern at 150 m (Figure 8), the springtime horizontal volume transports also support the BC narrows from Greenwich-Robert Islands to Nelson Island and widens downstream, contouring the bathymetry, towards King George Island.

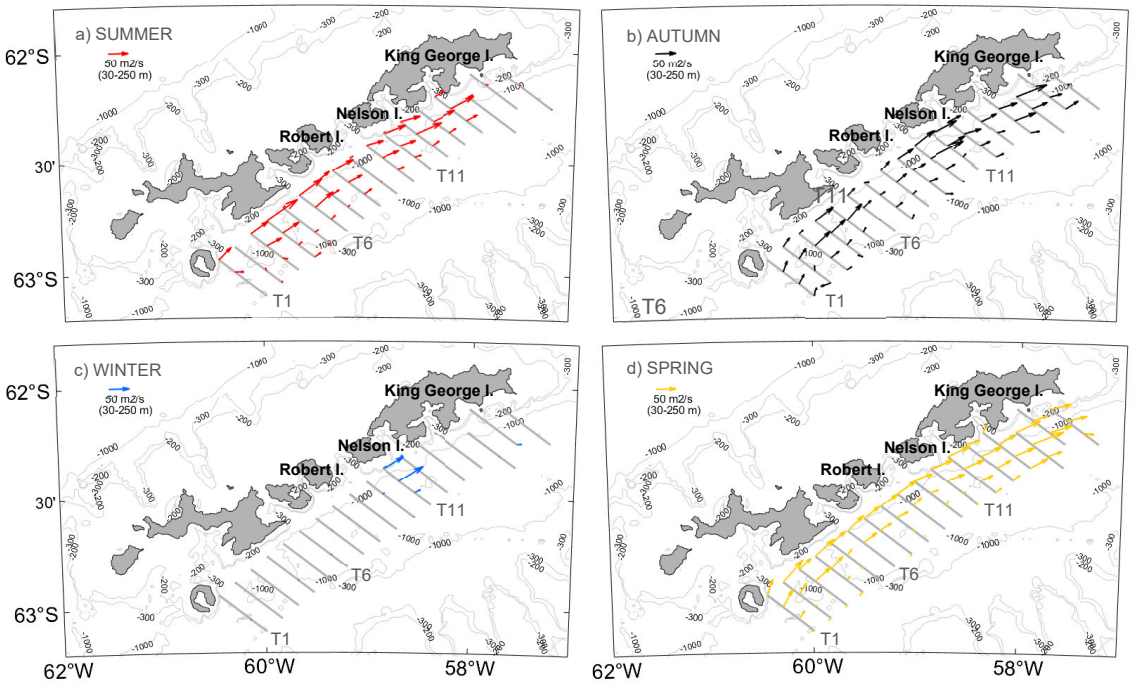

Figure 13. Map showing the transects of study and the associated seasonal horizontal transports (m^2/s) following a) summer, b) autumn, c) winter, d) spring. The four vectors along each transect originates from averaging the horizontal transport (m^2/s) driven by all available profiles and falling within each of the four cells of study (the closest to the island coastlines). The magnitude of the velocity field is scaled to the vector in the upper left corner of each panel.

4. DISCUSSION

We find the BC is present in all seasons (Figures 8, 11 and 13); velocity vertical profiles show its persistence even despite the scarcity of winter data (see Figure 7). Likewise, the seasonal horizontal distribution of integrated volume transports (30-250 m) shows the persistence of the BC flowing northeast along the southern slope of the SSI through all seasons. It is also noticeable that the BC displays a strong recurrence on its propagation towards to the northern region of the SSI. Moreover, the BC widens near the King George Island what might be related to the widening of the platform in this region.

Results show an apparent seasonal variability of the BC. BC velocities are lower at the Livingston-Robert Islands section closer to the SSI slope in autumn and winter (Figure

8). Differently, the BC path is more consistent as to velocity values during summer and spring seasons. Alongstream, the volume transport is noticeably higher from the Nelson Island to the north during summer and spring. We hypothesize this increase is likely due to the recirculation of the BC around the SSI, then returning partially to the main flow again between Robert and Nelson Islands. Regarding to autumn, data reveal different features of the BC. The current flows at higher velocities along Robert Island (transect 10) than along Nelson Island (transect 12). However, it also increases from King George Island to the northeast. This pattern might be explained if we consider that data represent an early autumn signal, so there could be an intense northern current contributing to the return flow. Furthermore, Sangrà et al. (2017) demonstrated this recirculation to the north during summer, once the BCS is established. We hypothesize that the recirculation of the BC might account for the increasing transport in autumn.

Finally, we find the BC leans on the SSI shelf slope in all seasons except for winter (Figure 11), when its core appears to move towards the center of the Strait and also when it reaches the highest winter velocities on record (>35 cm/s).

This offshore displacement of the BC core is observed in other seasons transects close to the channels between the islands. The intensification in autumn and the similarity in the summer and spring patterns (Figure 8) lead us to consider the possibility that the seasons in this region may have to be redefined, and that in fact the spring and autumn patterns correspond to early and late summer, respectively. This could account for the intensification observed in autumn, which might be the response to a well-established recirculation of BC likely crossing the Nelson Strait.

Table 2 summarizes the BC velocity and volume transport values found in the literature. Most of these studies are based on summertime measurements, so the description of the dynamic system set out in this introduction is valid only for that season, being unknown its persistence in other seasons. In these previous works, velocity values may be derived from direct measurements, or from hydrographic data, generally relative from the surface down to 500 db. Volume transports are also generally obtained by integrating the geostrophic velocities to 500 db. We note all these differences against year-round direct velocity measurements must be accounted for when comparing our climatological values and those referred to by other authors.

Grelowski et al. (1986) indicated that transport from Livingston to Nelson Island increases during spring-summer, but it decreases promptly arriving to King George Island. In our study, the transport distribution displays a similar pattern close to the coastline. However, this increases immediately after arrival to King George Island, reaching values similar to López et al. (1999). When comparing to transport estimated about 0.5 Sv provided by Gomis et al. (2002) along the southern slope of Livingston Island, we find our calculations for the volume transport reach nearly two times this value, U ~ 0.96 Sv (see Table 1). More recently, Savidge et al. (2009) reported transport estimates about 2 Sv at the eastern region of the Livingston Island, exceeding all reviewed values.

So far, the only published section crossing the Bransfield Strait with direct velocity measurements from Morozov (2007), while departing from Greenwich Island, reports a transport of 0.8 Sv in spring, a slightly higher value that our estimate of 0.56 Sv in Table 1. Lastly, we find that Sangrà et al. (2017) (their Figure 2) reported volume transports about 0.31-0.49 Sv for a transect nearly perpendicular to the channel in Nelson Strait. These values are relatively lower than our estimates for the same region and season, which are about 0.89 Sv and 0.52 Sv for summer and spring, respectively.

Table 2. BC velocity and transport estimates from the literature in the study region. The acronyms are: ADCP, Acoustic Doppler Current Profiler; CTD, Conductivity, Temperature and Depth; LADCP, Lowered Acoustic Doppler Current Profiler; RCM, Recording Current Meter; XBT, Expendable Bathythermograph; XCP, Expendable Current Profiler.

References	Magnitude (Velocity or transport)	Instrument	Methodology	Region	Data (month/year)
Grelowski et al., 1986	0.96 Sv 1.09 Sv 0.74 Sv	CTD	Geostrophic velocities relatives to 500 db	In front of (SSI) Livingston I. Nelson I. King George I.	12/1983 – 01/1984 (Spring – Summer)
Niiler et al., 1991	0.8 cm/s	CTD	Geostrophic velocities relatives to 200 db	Near western Deception I.	11/1986 – 03/1987 (Spring – Summer)
López et al., 1999	1 Sv	CTD + RCM (50, 300 and 700 m)	Geostrophic velocities relatives to 500 db	Near eastern King George I.	01 – 02/1994 (Summer)
Gomis et al., 2002	0.2 Sv 0.5 Sv	CTD	Geostrophic velocities relatives to 500 db	Inflow between Smith and Trinity I. In front of Livingston I.	12/1995 – 01/1996 (Spring – Summer)
Zhou et al., 2002	40 cm/s	Drifters at 15 and 40 m	Direct measures	Along the SSI slope	11/1988 – 01/1990 (Spring – Summer)
Zhou et al., 2006	40 - 50 cm/s	CTD / ADCP + Zhou et al., (2002) drifters	Direct measures and Geostrophic velocities relatives to 1000 db	Along the SSI slope	03/2004 (Summer)
Morozov, 2007	0.8 Sv	LADCP	Direct measures	In front of Greenwich I.	11/2005 (Spring)
Savidge et al., 2009	1 Sv 2 Sv	CTD + ADCP	Geostrophic velocities relatives to 500 db	Boyd Strait East of Livingston I.	1991-1997, 2001-2002 and 2003-2005 + 09/1999 – 12/2003 and 08/1997 – 09/2002 (Winter and Spring)
Sangrà et al., 2011	0.5 - 1 Sv	CTD	Geostrophic velocities relatives to 500 db	Along the SSI slope	12/1999 and 12/2002 – 01/2003 (Spring – Summer)
Poulin et al., 2014	30 - 40 cm/s	XCPs and ADCP	Direct measures and Geostrophic velocities relatives to 500 db	Between Robert and Nelson I.	01/2010 (Summer)
Sangrà et al., 2017	0.8 Sv	CTD + Argo drifters (50 and 100 m)	Direct measures and Geostrophic velocities relatives to 500 db	Along the SSI slope	01/2000 and 01/2010 (Summer)

Generally speaking, we find that the discussed estimates from previous works agree on the main with our results, while existing differences fall within the expected range of discrepancy due to a comparison where different methodologies apply and synoptic measurements are compared against climatological values. The above being said, there is a pattern which stands out consistently through all works, including the present study. During summer, the Bransfield Current System consists of a baroclinic jet flowing northeast and hugging the slope while contouring the bathymetry. This description ends with the recirculation of the BC to the north of the SSI as a result of the origin of the BC as a gravity current, a mechanism firstly posed by Sangrà et al. (2017). The climatological value of our results support further the recurrence of this pattern. As a second major finding of this work, we highlight the persistence of the BC as a northeastward-flowing jet all along the southern slope of the SSI, not only during summer but also during spring and autumn. We note that winter data scarcity prevents us from a similar statement during this season but still enables the confirmation of a strong northeastward-flowing current at least south off Nelson Island.

The lack of hydrographic data in our database does not allow us to confirm that beyond the summertime season, the BC carries water with TBW characteristics. However, taking into account the similarities between the patterns described for the BC in hydrographic works, and results from this research, we think one could reasonably argue that the summertime signal we report here as the BC is most likely carrying TBW properties. What water mass characteristics might be the BC driving during the other seasons through which we observe this jet is an open question to future research.

5. CONCLUSIONS

In this work we present the first seasonal climatology of the Bransfield Current System based on direct velocity measurements (SADCP data) collected between 1999 and 2014 through routinely repeated ship tracks from 275 cruises.

The main finding is the year-round persistence of the Bransfield Current, flowing northeastward along the SSI slope as a baroclinic jet with an approximate core width of 10-20 km and near-surface maximum velocities up to 30 cm/s. These results agree with the summertime view reported in previous works (Table 2) and support further that the BC flows as a coastal gravity current hugging the SSI slope and changing direction according to the bathymetry orientation. Furthermore, we observe that the core of the BC moves offshore at the wake of channels between islands.

Seasonally, the most distinctive difference is the recirculation of the BC around the northeasternmost tip of the SSI, which appears apparent in all seasons but during winter. This lack of recirculation during wintertime is, however, to be confirmed in the future given the present scarcity of data to confirm robustly its absence. This recirculation north of the SSI might be responsible of the BC flow strengthening observed at transects east

of the Nelson Strait, through which the recirculated BC might feedback itself within the Bransfield Strait.

The similarities between the climatological BC vertical structure and the observations reported in previous works lead us to suggest that the BC transports recurrently water with TBW characteristics during summer. However, the origin of the water masses transported during winter, along the same pathway, is yet unclear. To uncover this lack of knowledge in the future, year-round hydrographic measurements are demanding.

6. FUTURE WORK

The observational results discussed so far provide a seasonal climatological view of the Bransfield Current System. As a step forward, and having as reference these mean seasonal fields, we aim now to investigate the amplitude of interannual variations of the Bransfield Current System.

To this aim, we have identified through years all tracks that may act as transects routinely repeated in time over the same locations. This manner a more straightforward comparison between years is enabled (see an example of selected summer data in Figure 14). Lastly, we plan to combine these interannual velocity fields with in situ hydrographic data from concomitant cruises. This joint view will deliver the most comprehensive picture up to date of the Bransfield Current System based on observations.

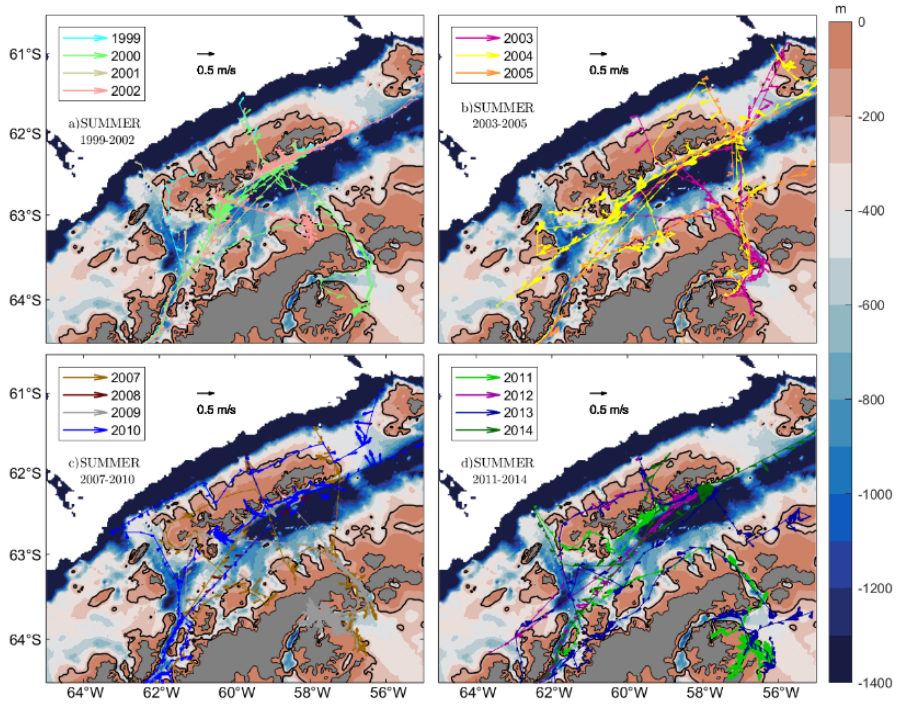

Figure 14. Horizontal maps showing summertime ship tracks in colours (solid lines) and selected for the study of interannual variations of the Bransfield Current. These tracks follow synoptic transects routinely repeated in time over the same locations. The coloured vector field indicated the current magnitude and directions through years (see legend). The different panels are showing different years: a) 1999-2002; b) 2003-2005; c)2007-2010; d)2011-2014. A scaled vector of 0.5 cm/s is added as reference.

7. REFERENCES

Basterretxea, G., & Arístegui, J. (1999). Phytoplankton biomass and production during late austral spring (1991) and summer (1993) in the Bransfield Strait. *Polar Biology*, *21*(1), 11-22.

Chelton, D. B., DeSzoeke, R. A., Schlax, M. G., El Naggar, K., & Siwertz, N. (1998). Geographical variability of the first baroclinic Rossby radius of deformation. *Journal of Physical Oceanography*, *28*(3), 433-460.

Ducklow, H. W., Baker, K., Martinson, D. G., Quetin, L. B., Ross, R. M., Smith, R. C., Stammerjohn, S. E., Vernet, M., & Fraser, W. (2007). Marine pelagic ecosystems: the west Antarctic Peninsula. *Philosophical Transactions of the Royal Society B: Biological Sciences*, *362*(1477), 67-94.

García, M. A., López, O., Sospedra, J., Espino, M., Gracia, V., Morrison, G., ... & Arcilla, A. S. (1994, September). Mesoscale variability in the Bransfield Strait region (Antarctica) during Austral summer. In *Annales Geophysicae* (Vol. 12, No. 9, pp. 856-867). Springer-Verlag.

García, M. A., Castro, C. G., Ríos, A. F., Doval, M. D., Rosón, G., Gomis, D., & López, O. (2002). Water masses and distribution of physico-chemical properties in the Western Bransfield Strait and Gerlache Strait during Austral summer 1995/96. *Deep Sea Research Part II: Topical Studies in Oceanography*, *49*(4-5), 585-602.

García-Muñoz, C., Lubián, L. M., García, C. M., Marrero-Díaz, Á., Sangrà, P., & Vernet, M. (2013). A mesoscale study of phytoplankton assemblages around the South Shetland Islands (Antarctica). *Polar biology*, *36*(8), 1107-1123.

Grelowski, A., Majewicz, A., & Pastuszak, M. (1986). Mesoscale hydrodynamic processes in the region of Bransfield Strait and the southern part of Drake Passage during BIOMASS-SIBEX 1983-1984. *Polish Polar Research*, *7*(4).

Hendry, K. R., Meredith, M. P., & Ducklow, H. W. (2018). The marine system of the West Antarctic Peninsula: status and strategy for progress.

Henley, S. F., Schofield, O. M., Hendry, K. R., Schloss, I. R., Steinberg, D. K., Moffat, C., Peck, L. S., Costa, D., Bakker, D. C. E., Hughes, C., Rozema, P. D., Ducklow, H. W., Abele, D., Stefels, J., Leeuwe, M. A. v., Brussaard, C. P. D., Buma, A. G. J., Kohut, J., Sahade, R., Friedlaender, A. S., Stammerjohn, S., Venables, H. J., & Meredith, P. G. (2019). Variability and change in the west Antarctic Peninsula marine system: Research priorities and opportunities. *Progress in oceanography*, *173*, 208-237.

Hewes, C. D., Reiss, C. S., & Holm-Hansen, O. (2009). A quantitative analysis of sources for summertime phytoplankton variability over 18 years in the South Shetland Islands (Antarctica) region. *Deep Sea Research Part I: Oceanographic Research Papers*, *56*(8), 1230-1241.

Hofmann, E. E., Klinck, J. M., Lascara, C. M., & Smith, D. A. (1996). Water mass distribution and circulation west of the Antarctic Peninsula and including Bransfield Strait. *Foundations for ecological research west of the Antarctic Peninsula*, *70*, 61-80.

López, O., García, M. A., Gomis, D., Rojas, P., Sospedra, J., & Sánchez-Arcilla, A. (1999). Hydrographic and hydrodynamic characteristics of the eastern basin of the

Bransfield Strait (Antarctica). *Deep Sea Research Part I: Oceanographic Research Papers*, *46*(10), 1755-1778.

Moline, M. A., Claustre, H., Frazer, T. K., Schofield, O., & Vernet, M. (2004). Alteration of the food web along the Antarctic Peninsula in response to a regional warming trend. *Global Change Biology*, *10*(12), 1973-1980.

Montes-Hugo, M., Doney, S. C., Ducklow, H. W., Fraser, W., Martinson, D., Stammerjohn, S. E., & Schofield, O. (2009). Recent changes in phytoplankton communities associated with rapid regional climate change along the western Antarctic Peninsula. *Science*, *323*(5920), 1470-1473.

Morozov, E. G. (2007, August). Currents in bransfield strait. In *Doklady Earth Sciences* (Vol. 415, No. 2, p. 984). Springer Nature BV.

Mulvaney, R., Abram, N. J., Hindmarsh, R. C., Arrowsmith, C., Fleet, L., Triest, J., ... & Foord, S. (2012). Recent Antarctic Peninsula warming relative to Holocene climate and ice-shelf history. *Nature*, *489*(7414), 141-144.

Niiler, P. P., Amos, A., & Hu, J. H. (1991). Water masses and 200 m relative geostrophic circulation in the western Bransfield Strait region. *Deep Sea Research Part A. Oceanographic Research Papers*, *38*(8-9), 943-959.

Lee, J. R., Raymond, B., Bracegirdle, T. J., Chades, I., Fuller, R. A., Shaw, J. D., & Terauds, A. (2017). Climate change drives expansion of Antarctic ice-free habitat. *Nature*, *547*(7661), 49-54.

Padman, L., Fricker, H. A., Coleman, R., Howard, S., & Erofeeva, L. (2002). A new tide model for the Antarctic ice shelves and seas. *Annals of Glaciology*, *34*, 247-254.

Poulin, F. J., Stegner, A., Hernández-Arencibia, M., Marrero-Díaz, A., & Sangrà, P. (2014). Steep shelf stabilization of the coastal Bransfield Current: Linear stability analysis. *Journal of physical oceanography*, *44*(2), 714-732.

Rintoul, S. R., Chown, S. L., DeConto, R. M., England, M. H., Fricker, H. A., Masson-Delmotte, V., Naish, T. R., Siegert, M. J., & Xavier, J. C. (2018). Choosing the future of Antarctica. *Nature*, *558*(7709), 233-241.

Sangrà, P., Gordo, C., Hernández-Arencibia, M., Marrero-Díaz, A., Rodríguez-Santana, A., Stegner, A., Martínez-Marrero, A., Pelegrí, J., & Pichon, T. (2011). The Bransfield current system. *Deep Sea Research Part I: Oceanographic Research Papers*, *58*(4), 390-402.

Sangrà, P., Stegner, A., Hernández-Arencibia, M., Marrero-Díaz, Á., Salinas, C., Aguiar-González, B., Henríquez-Pastene C., & Mouriño-Carballido, B. (2017). The Bransfield gravity current. *Deep Sea Research Part I: Oceanographic Research Papers*, *119*, 1-15.

Savidge, D. K., & Amft, J. A. (2009). Circulation on the West Antarctic Peninsula derived from 6 years of shipboard ADCP transects. *Deep Sea Research Part I: Oceanographic Research Papers*, *56*(10), 1633-1655.

Seyboth, E., Botta, S., Mendes, C. R. B., Negrete, J., Dalla Rosa, L., & Secchi, E. R. (2018). Isotopic evidence of the effect of warming on the northern Antarctic Peninsula ecosystem. *Deep Sea Research Part II: Topical Studies in Oceanography*, *149*, 218-228.

Talley, L. D., Pickard, G. L., Emery, W. J., & Swift, J. H. (2011). Section 9.8. 2.2 in Descriptive Physical Oceanography: An Introduction. Elsevier, Ch. 13 Southern Ocean, pp. 437-471

Tokarczyk, R. (1987). Classification of water masses in the Bransfield Strait and southern part of the Drake Passage using a method of statistical multidimensional analysis. *Polish Polar Research*, *4*(08).

Zhou, M., Niiler, P. P., & Hu, J. H. (2002). Surface currents in the Bransfield and Gerlache straits, Antarctica. *Deep Sea Research Part I: Oceanographic Research Papers*, *49*(2), 267-280.

Zhou, M., Niiler, P. P., Zhu, Y., & Dorland, R. D. (2006). The western boundary current in the Bransfield Strait, Antarctica. *Deep Sea Research Part I: Oceanographic Research Papers*, *53*(7), 1244-1252.

8. APPENDIX

Horizontal seasonal distributions at different depth ranges are shown in Figures 12-15. These distributions also illustrate BC features. BC can be detected in all seasons together with its baroclinity as depths get deeper.

Figure 15 shows the BC flow during summer. The BC is faster near the surface, reaching velocities higher than 25 cm/s all along the islands coastline and decreasing to less than 15-20 cm/s as one moves 20 km offshore. Recirculation of the BC is also noticeable at the northern tip of the SSI, rotating anticlockwise. Within the Bransfield Strait and off the BC, relatively weaker flow velocities towards the southwest are likely driven by the inflow of the Weddell Sea waters.

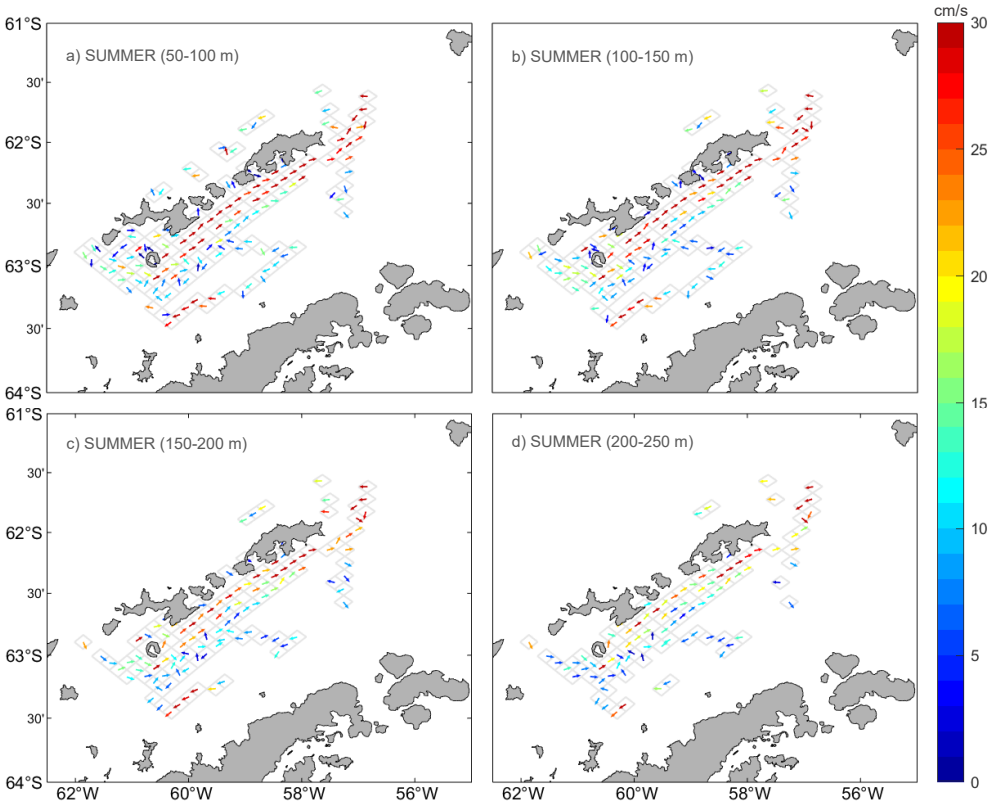

Figure 15. Horizontal distribution of summer velocities at different depths: a) 50-100 m, b) 100-150 m, c) 150-200 m, and d) 200-250 m.

In autumn (Figure 16), the BC displays a slightly different pattern with the strengthening of the jet occurring downstream of Robert Island, situated westward to the larger SSI Strait, while upstream the jet is weaker and less organized (a clear jet like-structure does not stand out). As expected, velocities of the BC also decrease at depth during this season. The recirculation of the BC around the SSI is still apparent as well as the soutwestward flow in the eastern basin.

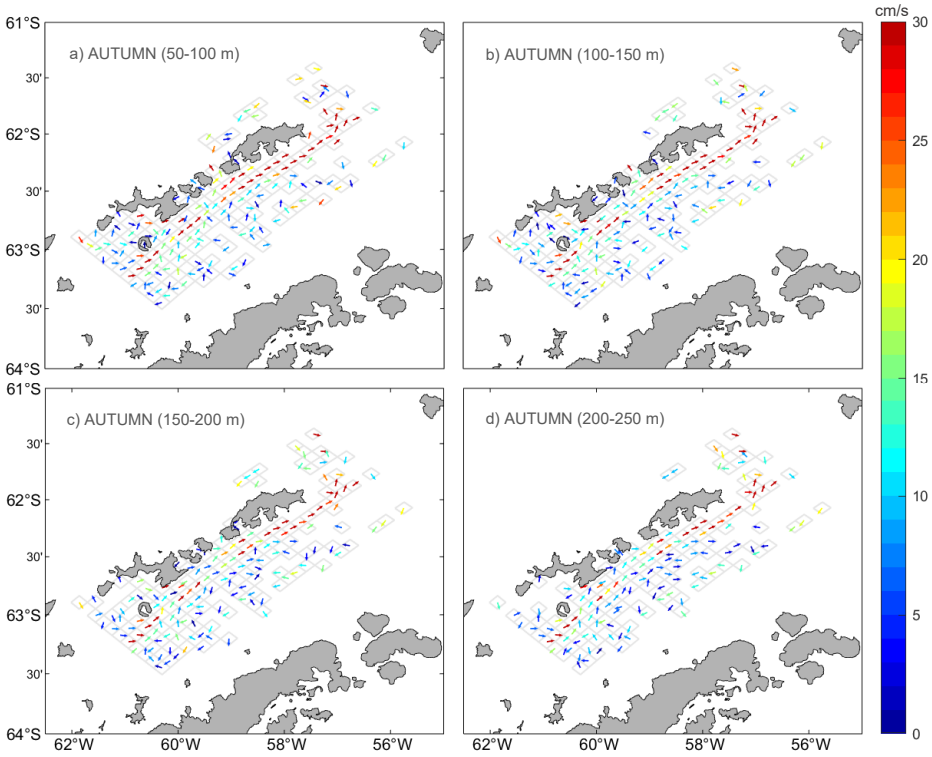

Figure 16. Same as Figure 15, but for autumn.

Through winter (Figure 17), scarcity of data hampers the view of the BC along its path; however, existing observations support the BC persists during this season, especially noticeable at the south of Nelson Island, eastward island of the larger SSI Strait. Importantly, the few winter data do not show the recirculation of the BC around the SSI.

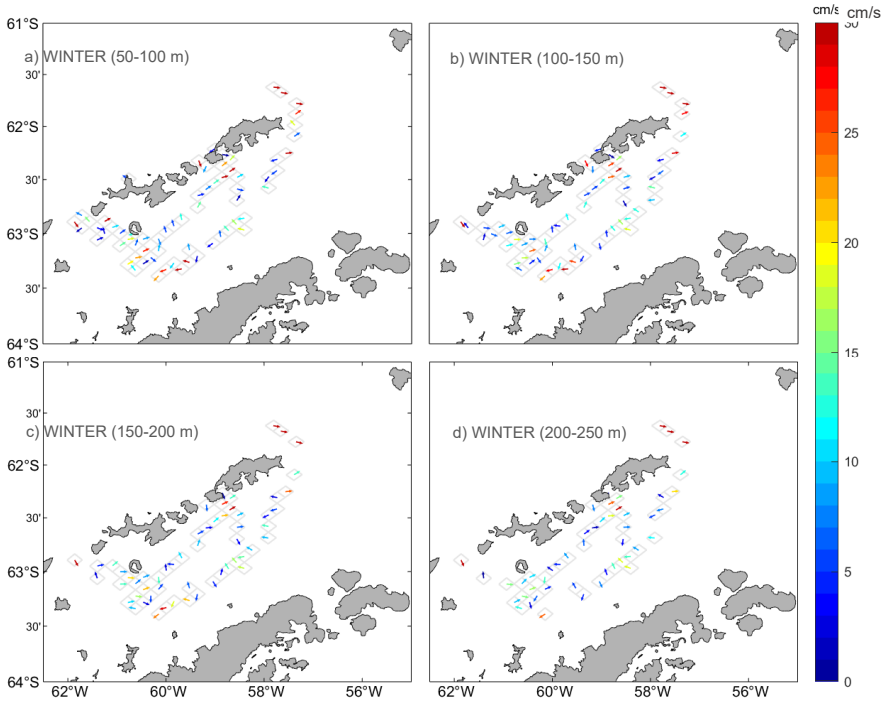

Figure 17. Same as Figure 15, but for winter.

During spring (Figure 18), we have the most comprehensive spatial view of the Bransfield Current System. All dynamic elements are visible: 1) the BC, flowing towards northeast from Deception Island to King George Island, and, then, 2) recirculating southwestward along the northern shelf of the islands; last, 3) a weaker and broader southwestward flow, occupying the middle and eastern side of the basin, likely driven by the inflow of Weddell Sea waters. During this season, the BC displays high velocities up to 30 cm/s all along its path, decreasing slowly at depth down to 250 m. Regarding its horizontal extent, the core of the BC is about 10-20 km wide from Deception Island to King George Island; downstream of the later, the BC widens up to 30 km before turning around the islands.

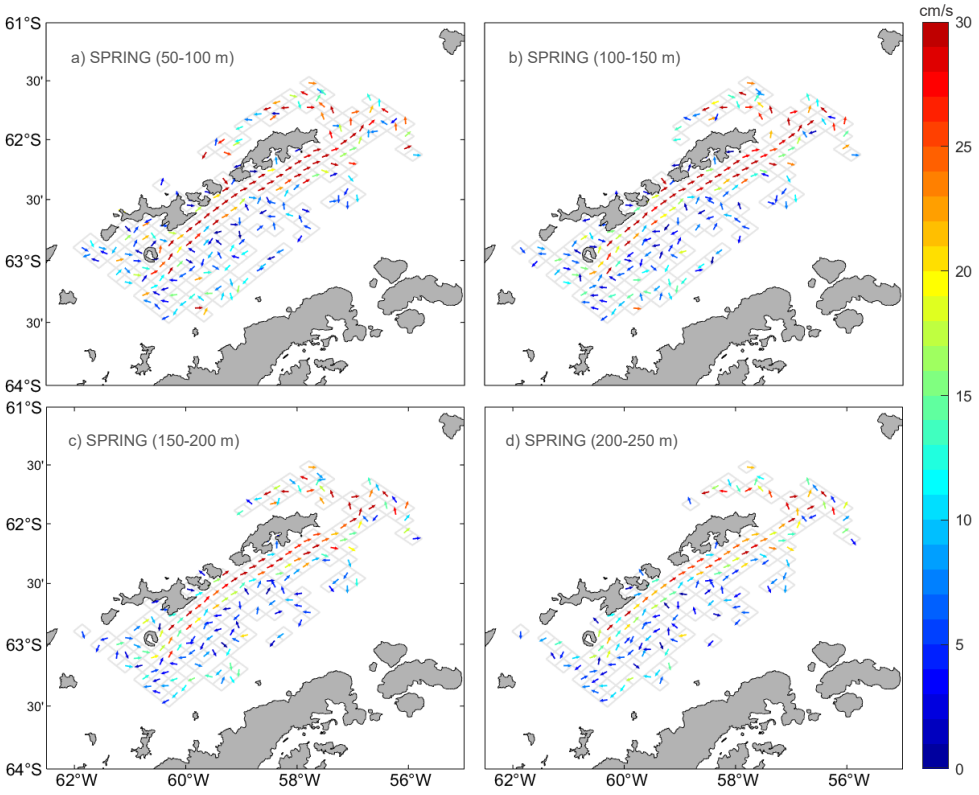

Figure 18. Same as Figure 15, but for spring.